The reaction pathway for the growth of alumina on high surface area alumina and in ultrahigh vacuum by a reaction between trimethyl aluminum and water

C. Soto and W. T. Tysoe[a)]
Department of Chemistry and Laboratory for Surface Studies, University of Wisconsin–Milwaukee, Milwaukee, Wisconsin 53211

(Received 26 November 1990; accepted 30 March 1991)

It is demonstrated that it is possible to grow thin alumina films on an alumina substrate by the sequential adsorption of water and trimethyl aluminum (TMA) both on high-surface-area alumina and in ultrahigh vacuum (UHV) at room temperature. The presence of the resulting layer is demonstrated on high surface-area substrates using infrared spectroscopy and in UHV using electron energy-loss spectroscopy (EELS). The correspondence between the reaction on high surface-area alumina and in UHV allow the surface species to be identified using infrared spectroscopy on the high surface-area sample, and the kinetics to be measured in UHV. A film formation reaction mechanism is proposed that is consistent with the experimental results. It is suggested that TMA can react with hydroxylated alumina to form an adsorbed dimethyl aluminum species and evolve methane. This can further react with water to evolve further methane and leave adsorbed methyl groups. These react rather slowly with water resulting finally in the formation of a hydroxylated alumina surface.

I. INTRODUCTION

Epitaxial, inorganic, thin films can be grown using a variety of strategies,[1] one of which, organometallic chemical vapor deposition (OMCVD) uses volatile, organic precursors. Commonly, the reactants for this growth scheme are alkyls of the metal and hydrides of the nonmetal.[2–12] These are invariably rather reactive and have fairly high vapor pressures, and react to form the inorganic compound and methane. The focus of this paper is an example of the latter reaction, that is, the reaction between trimethyl aluminum (TMA) and water. This reaction is chosen for a variety of reasons even though it is not entirely typical of OMCVD reactions that form III–V compounds.

(1) Aluminum trimethyl is a rather suitable reactant since it is thermally stable and does not pyrolize in the gas phase when heated to > 700 K, and therefore complications due to gas phase reactions are minimized.[13] It is a high-vapor-pressure (8.4 Torr) liquid at room temperature and is suitable for introduction into a ultrahigh vacuum (UHV) chamber[14] and is easy to obtain with high purity.[15]

(2) The reaction between trimethylaluminum (TMA) and water is highly exothermic having an enthalpy of reaction of -297.2 kcal/mole, thus optimizing the chance of carrying out the reaction under ultrahigh vacuum conditions.[16]

(3) Pressed pellets of high surface area alumina can be made for infrared analysis of adsorbed species, and a significant amount of work has already been carried out to identify adsorbed species following metal alkyl adsorption on both silica[17–20] and alumina.[21]

(4) The adsorption of water on alumina and the resulting surface species are well understood.[22–28]

The majority of fundamental studies of thin film formation from volatile organometallic precursors have focused on the growth of metal films rather than the reactive growth of inorganic layers. Examples of metallic film growth are the deposition of aluminum from various aluminum-containing organics,[29–34] deposition of tungsten films from tungsten hexafluoride,[35,36] and metal films from the decomposition of volatile metal carbonyls.[37,38] This work, in contrast, focusses on the formation of thin films formed by reaction between two adsorbed species, namely trimethyl aluminum and water.

Apart from continuous growth of thin inorganic films by a steady-state reaction between a metal alkyl and a hydride, a technique known as atomic layer epitaxy (ALE) has been developed where thin films of extremely well-controlled thickness can be deposited by sequential application of each of the reactants[39–44] so that films are grown in a layer-by-layer fashion. This experimental strategy is taken as the basis of this work to form thin alumina films and to scrutinize the film deposition reaction pathway by sequentially depositing TMA and water to grow the film.

Thus, it is demonstrated in the following that the reaction between TMA and water is sufficiently exothermic that thin alumina films can be grown using exposures attainable in ultrahigh vacuum (UHV) and at room temperature. Identification of complex reaction intermediates using current surface-sensitive techniques is difficult, although ultraviolet photoelectron spectroscopy (UPS)[45] and high-resolution electron energy-loss spectroscopy (HREELS)[46] have shown some promise. However, the growth of thin films by sequential TMA and water adsorption observed in UHV has been duplicated using high surface area alumina substrates. This allows any surface reaction intermediates to be examined using high resolution infrared spectroscopy.[17–21]

The experiments described in the following demonstrate that aluminum trimethyl reacts with hydroxylated alumina even at room temperature. Further addition of water, also at room temperature, results in the complete decomposition of

 0734-2101/91/052686-10$01.00

$Al(CH_3)_3$-derived surface species and the recovery of the original hydroxylated surface. That is, it is possible to grow a layer of alumina by sequential deposition of aluminum trimethyl and water. In addition, the coupling of results on high surface-area substrates and UHV allows unique insights to be gleaned into the nature of the surface reaction intermediates as well as detailed measurements of the reaction kinetics to be obtained in a way which would not be possible in the individual experiments.

II. EXPERIMENTAL

A. Infrared spectroscopy

Infrared spectra were obtained using the apparatus shown in Fig. 1. A ~0.1-mm thick, pressed pellet of high surface area γ-alumina is supported in a wire cage attached to the end of a glass rod. The alumina has a surface area of ~120 m^2/g after formation of the pellet. A piece of iron is sealed into the end of the glass rod so that the sample can be extended and retracted using a magnet. The end of the cell is fitted with infrared transmitting windows (sodium chloride, 5-mm thick) to allow infrared spectra of the alumina pellet to be obtained. The sample can also be retracted into a furnace that can be heated to 800 K. Temperature measurement is by means of a chromel/alumel thermocouple inserted into the furnace material. The temperature is controlled by means of a Eurotherm temperature controller which is capable of controlling to $\pm$ 1 K. Glass bulbs are also attached directly to the infrared cell to allow reactant introduction. In the case of these experiments, the bulbs contained TMA and water or D_2O. The reactants were purified by several freeze/thaw cycles under vacuum, and the gas purities were monitored using infrared spectroscopy. The purities of these reactants prepared using an identical protocol were also analyzed mass spectroscopically (see below) which confirmed that the purification cycle indeed produced pure compounds. The infrared cell was attached to a portable, liquid-nitrogen-trapped diffusion pump which is capable of evacuating the cell to ~2×10^{-6} Torr. Pressure measurements in this case was by means of a cold cathode ionization gauge attached to the portable pumping apparatus.

Infrared spectra were obtained using a Mattson MX-1 Fourier transform infrared spectrometer operating at 1 cm^{-1} resolution. Spectra were obtained using 600 accumulation cycles which resulted in spectra displaying very low signal to noise ratios.

The pellets were prepared from γ-alumina powder (Aksochimie, 187 m^2/g), and pressed between steel anvils at 2000 psi resulting in pellets of approximately 0.1 mm in thickness. The pellet was inserted into the infrared cell, which was evacuated to 2×10^{-6} Torr, and the pellet retracted into the furnace and heated to 800 K to remove any surface contaminants. The sample was allowed to cool to room temperature and exposed to water (20 Torr, 300 s) in order to hydroxylate the surface.

B. Ultrahigh vacuum apparatus

The 12 in. diam, stainless-steel ultrahigh vacuum (UHV) apparatus used for these experiments is pumped by means of an ion pump and titanium sublimation pump and operates at a base pressure of 2×10^{-10} Torr following bakeout. It is equipped with a rotatable, carousel geometry manipulator capable also of x, y, and z motion. The aluminum foil used for these experiments (99.999%, Aldrich Chemicals) is spot welded to tantalum posts. In order to facilitate the spot welding, the portion of the aluminum attached to the post is sandwiched between pieces of tantalum foil. The sample can be resistively heated and temperature measurement is by means of a chromel/alumel thermocouple spot welded to a tantalum foil pad attached to the rear of the foil. The chamber is also equipped with a mass spectrometer for leak testing, residual gas analysis and thermal desorption spectroscopy. The spectrometer is capable of monitoring up to five masses simultaneously as a function of time. The mass spectrometer is enclosed in a stainless steel shroud with a 1-cm diam opening in front of the ionizer of the mass spectrometer. The rear of the shroud incorporates pump-out holes so that the spectrometer is effectively evacuated. The sample can be rotated so that it is located in front of the hole in the mass spectrometer shroud for thermal desorption spectroscopy,

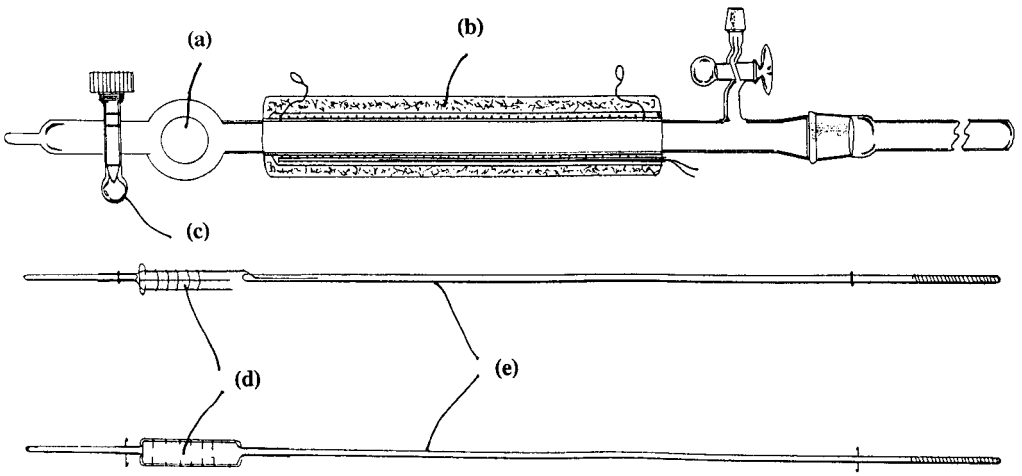

FIG. 1. A schematic diagram of the infrared cell used to obtain spectra of trimethyl aluminum- and water-derived surface species adsorbed on high-surface-area alumina showing (a) the infrared window, (b) the furnace, (c) the reactant reservoir, (d) the pellet holder at the end of (e) the sample transfer rod.

and is 2 mm away from the hole. This ensures that species evolving from the front face of the sample only are detected. The aluminum sample was cleaned using a standard protocol.[28,47] By annealing *in vacuo* for 1 h at ~700 K, and then argon-ion bombarding (1500 eV; 4 μA/cm^2) at room temperature for 5 min. This procedure was repeated until no contaminants, primarily oxygen and carbon, were detected using Auger spectroscopy.

The chamber contains a retarding field analyzer (RFA) which is used for Auger and electron energy loss experiments, and can also be used for low energy electron diffraction experiments in the case that a single crystal is used. Auger spectra are excited using a grazing incidence (10°) electron gun operating at 2 kV. Electron energy-loss (EELS) spectra are excited using a normal incidence electron gun operating at 355 eV.

Gases are introduced into the chamber either by back filling via a leak valve or through a directional doser consisting of a 1-cm diam stainless-steel tube. In the latter case, the sample can be rotated so that the reactant is incident directly onto the front face of the sample. The leak valves are connected to an all-glass gas-handling line that is pumped to 1×10^{-7} Torr by means of a liquid-nitrogen-trapped diffusion pump.

The TMA (Aldrich Chemicals, 97%) was transferred to a glass vial, and the D_2O (Sigma Chemicals, 99.8%) was removed using a syringe via the septum into the glass container which was immediately sealed to minimize water contamination. The reactants are outgassed using repeated freeze/thaw cycles. The purities of the gases are monitored using mass and infrared spectroscopies.

III. RESULTS

A. Ultrahigh vacuum experiments

The clean aluminum foil was oxidized at 773 K in 3×10^{-6} Torr of oxygen for 3 min to form a thin oxide layer.[27,28,48] The resulting oxide was then exposed to 600 L (1 L = 1×10^{-6} Torr s) of water at a sample temperature of 300 K in order to hydroxylate the surface.[51] Note that exposures are uncorrected for ionization gauge sensitivities. Figure 2 shows a plot of the carbon Auger signal at 273 eV kinetic energy, measured from the peak-to-peak amplitude in the spectrum, normalized to the oxygen substrate Auger signal [designated C(273)/O(520)] as a function of trimethyl aluminum exposure at room temperature (300 K) with the sample placed in front of the dosing source. Clearly, TMA adsorbs onto the hydroxylated alumina sample at 300 K. Pressure measurements in these experiments is by means of a nude ionization gauge located in the vacuum chamber and these exposures do not take account of pressure enhancements in the directional doser. Calibration experiments carried out by monitoring the methane thermal desorption signal from a palladium (111) single crystal obtained both by dosing the sample by back filling the chamber and via the directional doser indicate that the doser has an enhancement factor of 8 ± 1. It is clear that, although TMA does adsorb onto the hydroxylated alumina sample, the sticking probability is relatively low since the surface has not completely saturated even after an exposure (corrected for the dosing source enhancement factor) of greater than 2000 L. The saturation Auger ratio after adsorption of TMA on hydroxylated alumina is 1.85 ± 0.05 (Fig. 2). The corresponding ratio of C(273)/O(520) after saturating an alumina surface that had not been pre-exposed to water was 3.5 ± 0.2.

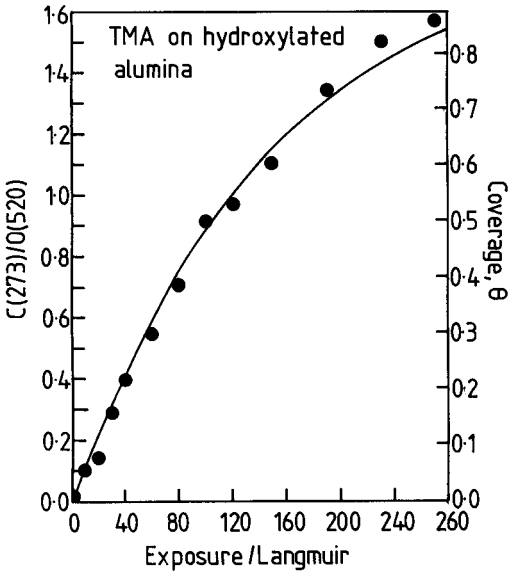

FIG. 2. Plot of the ratio of the peak-to-peak amplitude of the carbon *KLL* Auger transition at 273 eV kinetic energy to the intensity of the oxygen *KLL* transition at 520 eV kinetic energy, C(273)/O(520), as a function of trimethyl aluminum exposure (●). Plotted as a solid line on the experimental data is the result of a theoretical fit assuming adsorption via Langmuir kinetics.

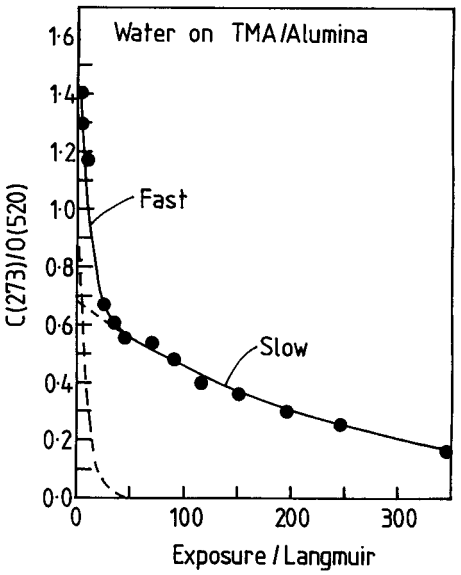

FIG. 3. Plot of the C(273)/O(520) Auger ratio as a function of water exposure to a trimethyl aluminum-covered surface (●). Plotted as a solid line on the experimental data is a theoretical fit assuming a fast and a slow trimethyl aluminum removal rate. The individual rates are shown as dashed lines.

This surface was then exposed to water by back filling the chamber rather than using the dosing source. This was done to avoid contamination of the portion of the gas line and dosing source that was used for TMA. The resulting plot of C(273)/O(520) is shown in Fig. 3, and clearly demonstrates that carbon is reactively removed from the surface by reaction with water at 300 K. Note that during these experiments, the oxygen signal also grew slightly indicating additional adsorption of oxygen onto the surface. The carbon Auger signal drops precipitously with exposure up $\sim$50 L, and then decreases significantly more slowly with water exposure thereafter.

Following almost complete removal of the surface carbon by reaction with water, the surface was re-exposed to TMA reproducing the curve of Auger ratio [C(273)/O(520)] displayed in Fig. 2, and again this carbon could be reactively removed by water. This procedure could be reproducibly repeated several times.

It should be mentioned that the carbon signals are normalized to the substrate oxygen signal rather than the aluminum signal since the low kinetic energy of the aluminum *LMM* Auger transition (60–80 eV) necessitated decreasing both the modulation amplitude and incident current to detect it using the RFA. This results in a significant deterioration of the signal-to-noise and is therefore less suitable for quantitative measurements.

Figure 4 shows the electron energy-loss (EELS) spectra of the sample, following various pretreatments, collected using 355 eV electrons displayed as the first derivative. The zero of energy in the spectrum is taken to be the maximum negative excursion in the first derivative of the primary peak. The spectrum displayed in Fig. 4(a) is of the clean aluminum surface. The loss features are due to both surface and bulk plasmon losses. The peak positions measured in this experiment are shown in Table I and compared with data from Ref. 49.

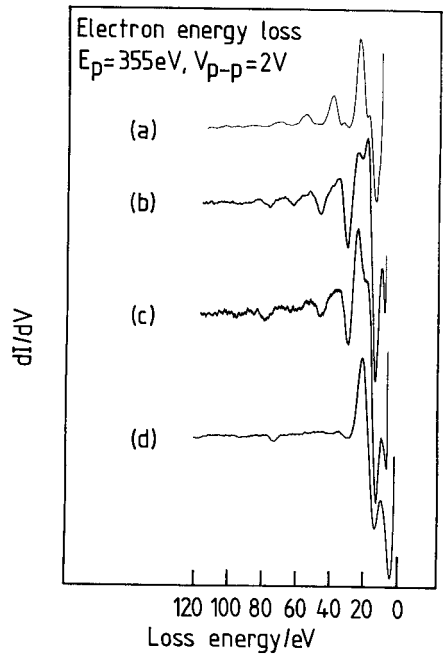

FIG. 4. A series of electron energy-loss spectra plotted in derivative mode taken using an incident electron energy of 355 eV at normal incidence. (a) the clean aluminum surface; (b) following oxidation using 600 L of O_2 at 773 K; (c) after exposure of the oxidized aluminum surface to 600 L of water; (d) after alumina deposition using four sequential adsorption cycles of trimethyl aluminum and water.

TABLE I. Table showing the loss energies for a clean aluminum surface taken from Ref. 49 compared with the results from this work.

Loss energy/eV, Ref. 49	Loss energy/eV, this work
10	13
15	19
25	30
30	35
41	45
45	
55	62
62	
78	79

Oxidation of the sample in 2×10^{-6} Torr of O_2 (using an exposure of 600 L) at 773 K produces the loss spectrum shown in Fig. 4(b). The loss energies obtained from this spectrum are shown in Table II and compared with the results of Olivier and Poirier.[50] Peak assignments taken from the work of Olivier and Poirier are also shown in Table II. Clearly the agreement between the two spectra is good indicating that a surface oxide has indeed formed. Exposing this surface to 600 L of water at 300 K yields the spectrum shown in Fig. 4(b), which is essentially identical to that of the oxidized surface [Fig. 4(c)] except that the peak intensities at

TABLE II. Table showing the energies of the loss features taken from Ref. 50 compared with the energies obtained in this work. Also shown are the assignments of the features taken from Ref. 50.

Loss energy/eV, Ref. 50	Loss energy/eV, this work	Assignment
9.2	8	Exciton
16.5	14	Interband transitions
20.7	22	
30.3	30	O 2*s* interband transition
46	46	O 2*s* interband transition
62	62	O 2*s* interband transition
...	76	Al 2*p* interband transition

62 and 22 eV loss energies are attenuated. Figure 4(d) shows the loss spectrum obtained following four TMA + water deposition cycles, finishing with water exposure (so that the surface exhibited no carbon Auger signal).

B. Infrared spectroscopy of reaction intermediates on alumina

Reactions where alumina is deposited by sequential TMA and water exposures can be reproduced on high-surface-area alumina. In this case, infrared spectroscopy is used to establish the nature of the surface intermediates that are formed. As mentioned above, alumina is ideally suited for these experiments since it can be obtained with high surface area, displays a wide infrared window (with a cutoff below ~ 1200 cm^{-1}), and the OMCVD reaction to form alumina is very exothermic.

Figure 5(a) shows the infrared spectrum of the hydroxylated alumina pellet, which displays a broad, asymmetric peak centered at ~ 3400 cm^{-1} due to hydrogen-bonded surface hydroxyl groups and is consistent with the pretreatment procedure.[22–26] The large shoulder below ~ 1200 cm^{-1} is due to absorption by the alumina lattice modes and the small peaks between 1200 and 1400 cm^{-1} are due to a small amount of remaining, unreacted water at the surface. The base line of the spectrum also increases with frequency due to scattering of the infrared radiation from the small alumina particles.

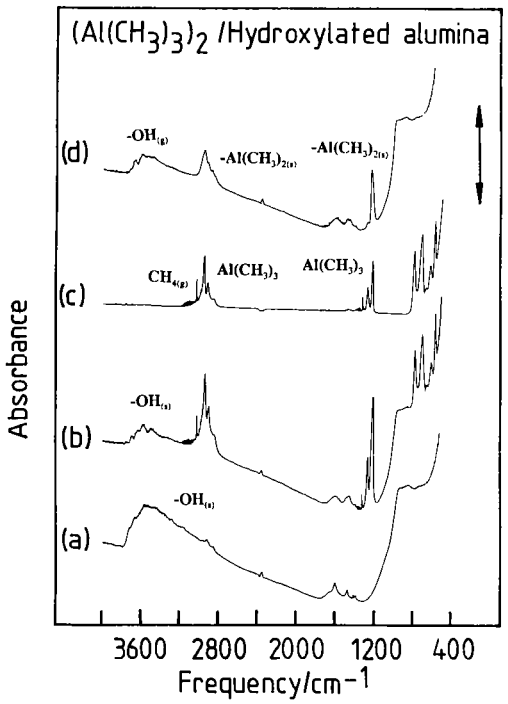

FIG. 5. A series of infrared spectra collected following the exposure of an alumina pellet to trimethyl aluminum (TMA). (a) spectrum of the hydroxylated γ-alumina pellet; (b) spectrum of the gas-phase and surface species obtained following exposure of TMA; (c) spectrum of the gas phase obtained by removal of the pellet from the infrared beam; (d) spectrum of the pellet obtained by evacuating the infrared cell. Peak assignments are marked adjacent to the spectral features as discussed in the text.

This sample is then exposed to 10 Torr of trimethyl aluminum for 60 s at room temperature. Spectrum 5(b) is obtained following this treatment, and shows both the surface and the gas-phase contributions to the spectrum. The spectrum of the gas phase alone obtained by moving the alumina pellet out of the infrared beam using exactly identical experimental conditions is displayed in Fig. 3(c). The broad peaks at ~ 3000 cm^{-1} are assigned to methyl stretches and peaks between 1200 and 700 cm^{-1} are due to methyl bending modes.[52] Finally, peaks below 600 cm^{-1} are due to skeletal modes of TMA and indicates the presence of dimeric aluminum trimethyl, $Al_2(CH_3)_6$. Note, however, that nuclear magnetic resonance (NMR) spectroscopy indicates that the methyl groups in the dimer can exchange rapidly at room temperature since two peaks due to terminal or bridging methyl groups are detected only following cooling to ~ 200 K.[51]

The presence of remaining gas-phase TMA suggests that the alumina surface is completely saturated. In addition to the peaks due to TMA, sharp peaks are evident at 3400 and 1300 cm^{-1} (along with the associated *P* and *R* rotational bands), which are ascribed to the presence of gas-phase methane.[53] Figure 5(d) shows the spectrum of the alumina pellet following exposure to TMA and after evacuating the cell to remove gas-phase products. Note, that the addition of spectra 5(c) and 5(d) essentially reproduces the spectrum in Fig. 5(b) indicating that the surface is not modified by evacuating the cell. The peaks in the hydroxyl stretching region (3500 cm^{-1}) are attenuated by TMA addition, indicating that the trimethyl aluminum has reacted with surface hydroxyls to evolve methane. The resulting surface species exhibits peaks at ~ 2900 cm^{-1} in the CH stretching region of the spectrum and at ~ 1150 cm^{-1} in the CH bending region of the spectrum indicating that methyl groups are still present on the surface. The nature of this surface species will be discussed in greater detail below.

This surface is then exposed to D_2O at room temperature (300 K), and the resulting spectrum, obtained after evacuating any gas-phase products, is shown in Fig. 6(a). A broad, asymmetric feature is evident centered at ~ 2400 cm^{-1}, and is due to surface deuteroxyl groups which are shifted due to the change in reduced mass of the surface species. The features in the CH stretching region at ~ 2900 cm^{-1} are attenuated but not completely eliminated, and the peak positions in this region are different to those displayed in Fig. 5(d). Figure 6(b) shows the corresponding gas-phase spectrum obtained by moving the pellet out of the path of the infrared beam. The spectral features, in this case, correspond exactly to the infrared spectrum of CH_3D,[53] indicating that the D_2O has reacted with a portion of the methyl groups remaining at the surface. Carrying out this final step using H_2O rather than D_2O allows a quantitative comparison to be made, using the infrared absorbences, of the amount of methane released from the surface by the addition of TMA to a hydroxylated surface and that evolved by subsequent addition of water and shows that essentially equimolar amounts of methane (within 5%) are released in each step. Further addition of TMA results in the spectrum shown in Fig. 6(c), where the OD peak is attenuated and the peaks in

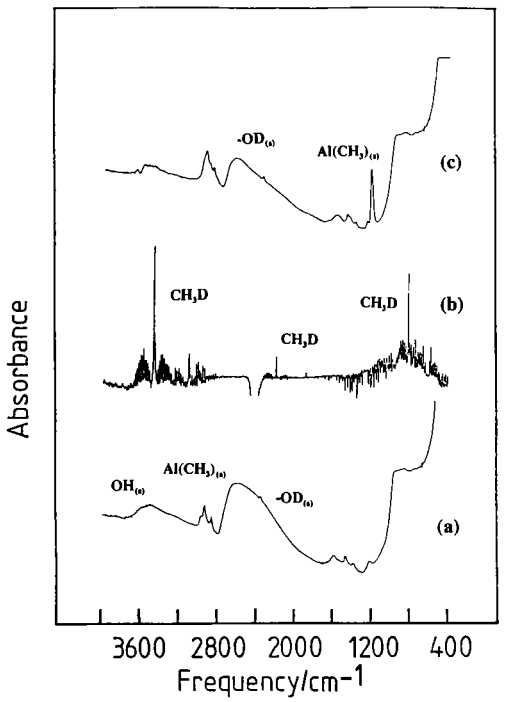

FIG. 6. A series of infrared spectra obtained after exposure of a TMA-covered surface to D_2O. (a) spectrum of the surface after evacuation of gas-phase products; (b) infrared spectrum of the gas phase obtained by moving the sample out of the infrared beam; (c) spectrum of the surface obtained by re-exposure to TMA. Peak assignments are marked adjacent to the spectral features as discussed in the text.

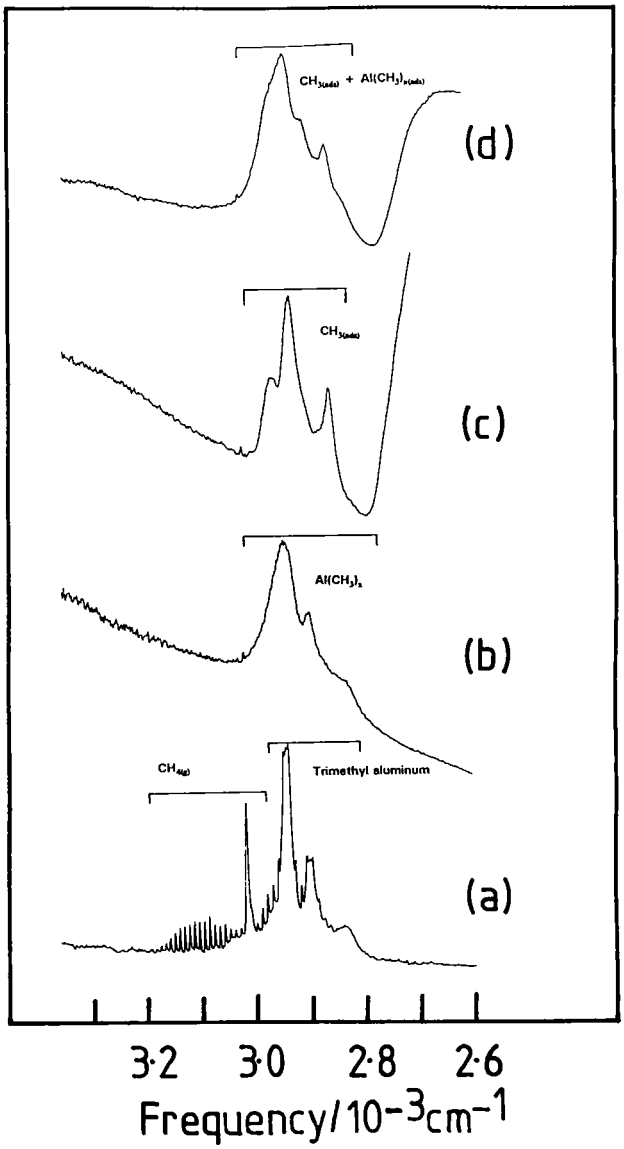

FIG. 7. A series of infrared spectra obtained in the CH stretching region between 2600 and 3500 cm^{-1} showing (a) the spectrum of gas-phase trimethyl aluminum and methane; (b) the surface species obtained by exposing hydroxylated alumina to TMA and evacuating the cell; (c) the surface species found after exposing a TMA-covered surface to D_2O and evacuating the cell; (d) the spectrum obtained by exposing the surface whose spectrum is shown in (c) to further TMA. Peak assignments are marked adjacent to the spectral features as discussed in the text.

the CH stretching region grow. No peaks are observed due to C–D stretches indicating that there is no H–D exchange between the surface methyl and hydroxyl groups. This view is corroborated by the presence of only CH_3D following the addition of D_2O.

Figure 7 shows a series of spectra in the CH-stretching region following various treatments (expanded from the data in Figs. 5 and 6). Figure 7(a) shows the spectrum displayed between 2600 and 3500 cm^{-1} showing features due to gas-phase species formed by reaction of TMA with hydroxylated alumina taken from the spectrum shown in Fig. 5(c). Clearly visible is the T_1 mode of methane at 3016 cm^{-1} along with the rotational wings. The three broader peaks are assigned to CH stretching modes of the methyl group of TMA. The peak at 2950 cm^{-1} is assigned to the symmetric stretch, the peak at 2902 cm^{-1} to the asymmetric methyl stretch, and the broad peak at 2850 cm^{-1} to an overtone of a methyl wagging mode. Note that the overtone and the asymmetric stretch are coupled, and therefore shifted, by a Fermi resonance.[53–55] The spectrum shown in Fig. 7(b) is of the surface species obtained by exposing a hydroxylated surface to TMA [taken from spectrum 5(d)], and displays peaks at 2943, 2900, and 2830 cm^{-1} similarly assigned to symmetric and asymmetric stretches and an overtone respectively, the latter modes also coupled via a Fermi resonance. The similarity between this spectrum and that due to TMA strongly suggests the presence of an $Al(CH_3)_x$ surface species. The detection of gas-phase methane implies that $x < 3$. The nature of this species will be discussed in greater detail below.

Figure 7(c) shows the CH-stretching spectrum of the surface species formed after exposure of a TMA-covered surface to D_2O [taken from spectrum 6(a)], and exhibits peaks at 2960, 2928, and 2856 cm^{-1}. Note that the integrated intensity of this peak is $50 \pm 5\%$ of that shown in Fig. 7(b). Finally, shown in Fig. 7(d) is the spectrum obtained by exposing the surface displaying the spectrum shown in Fig. 7(c) to further TMA. This spectrum can be reproduced by adding spectrum 7(b) and 7(c).

This reaction sequence can be repeated several times, and each time reproduces the spectrum of the original alumina

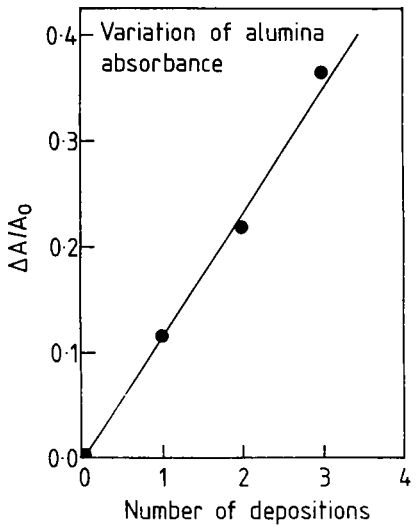

FIG. 8. Plot of the alumina absorbance as a function of the number of sequences of TMA and water adsorption (●).

pellet. In order to confirm that aluminum oxide is indeed being deposited by the above sequential reaction between $Al(CH_3)_3$ and water, the following experiment was carried out. A hydroxylated surface was exposed to trimethyl aluminum, evacuated, further exposed to water to regenerate the original surface without changing the position of the sample and an infrared spectrum of the pellet recorded. This procedure was repeated several times, again without altering the position of the pellet.

First, the absorbance of the pellet in the region assigned to Al_2O_3 (below 1200 cm^{-1}) is measured after each deposition cycle. Shown in Fig. 8 is the change in absorbance (ΔA) normalized to the absorbance of the initial pellet (A_0), plotted as a function of the number of alumina deposition cycles. Clearly, the absorbance increases with each deposition cycle, indicating that alumina is indeed being deposited on the pellet.

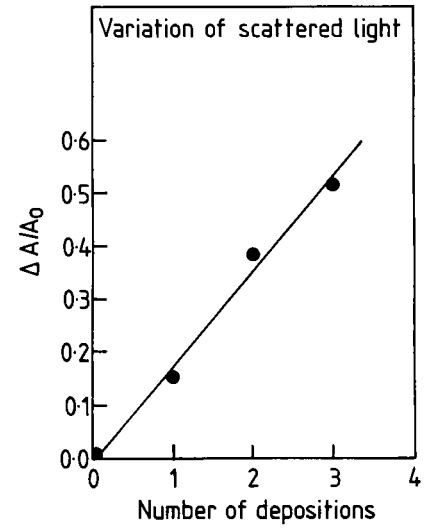

FIG. 9. Plot of the background intensity due to light scattering as a function of the number of sequences of TMA and water adsorption (●).

Further confirmation of the deposition of alumina by the sequential reaction of TMA and water is given by the data of Fig. 9. In this case the variation in scattered light, measured from the height of the base line at 3800 cm^{-1} (ΔS) normalized to the scattering due to the initial pellet (S_0) is shown plotted as a function of the number of deposition cycles. Since the scattering cross section increases linearly with the volume of the particle[56] (at least, when the particle size is much smaller than the wavelength of the scattering radiation), this suggests an increase in particle size as deposition proceeds. These results indicate that an alumina film can be deposited by a sequential reaction of TMA and water. The growth protocol used here is identical to that used to grow thin alumina films using a technique known as atomic layer epitaxy (ALE) where an approximately 1-Å thick film grows during each deposition cycle.[57]

IV. DISCUSSION

Both infrared (Fig. 5) and Auger spectroscopy (Fig. 2) show that trimethyl aluminum adsorbs onto hydroxylated alumina. The infrared data [Fig. 5(c)] indicate that adsorption is accompanied by methane evolution. The larger value of C(273)/O(520) observed following TMA adsorption onto unhydroxylated alumina (3.5 ± 0.2) compared to adsorption onto the hydroxylated surface (1.85 ± 0.05) implies that a portion of the carbon in TMA is reactively removed during adsorption onto the hydroxylated surface in accord with the observation that methane in formed by this reaction in the infrared experiments.

The shape of the uptake curve in Fig. 2 suggests that the TMA sticking probability decreases with coverage and can be modeled using Langmuir kinetics[58]:

$$S = S_0(1 - \Theta), \tag{1}$$

where S is the sticking probability, S_0 the sticking probability at zero coverage, and Θ is the coverage such that saturation corresponds to $\Theta = 1$. Since $S = Kd\Theta/dE$ where E is the exposure and K is a constant, which depends on the number of adsorption sites per unit area and the collision frequency of the adsorbate, the coverage can be written as a function of exposure as:

$$\Theta = [1 - \exp(-S_0E/K)] \tag{2}$$

Shown plotted as a solid line on the data of Fig. 2 is a curve of this type assuming that Θ is proportional to the carbon Auger signal, where $S_0/K = 0.35 \pm 0.05$ $Torr^{-1}\,s^{-1}$. Clearly the fit is good suggesting that TMA adsorbs onto hydroxylated alumina via first-order (one site) Langmuir kinetics. This implies that TMA loses a single methyl group to interact with a single surface hydroxyl group to form $Al(CH_3)_{2(ads)}$. Note that reaction with two adjacent surface hydroxyl groups forming $Al(CH_3)_{(ads)}$ would yield two-site adsorption kinetics and a sticking probability proportional to $(1 - \Theta)^2$.

By calculating the collision frequency for TMA per unit area at room temperature and assuming approximately 1×10^{15} adsorption sites/cm^2 on the alumina surface a reac-

tion probability for a TMA molecule with a hydroxylated alumina surface of $\sim 10^{-2}$ is obtained; that is only approximately 1% of the incident TMA molecules adsorb.

The infrared spectrum of the corresponding surface species is shown in Fig. 5(d), and an expanded spectrum of the methyl stretching region is shown in Fig. 7(b). The latter spectrum displays peaks at 2943, 2900, and 2830 cm^{-1}. These frequencies are very close to the methyl stretching frequencies for TMA itself which displays modes at 2940, 2900, and 2838 cm^{-1} and implies a surface species substantially similar to TMA. A spectrum with essentially identical vibrational frequencies (at 2940, 2900, and 2830 cm^{-1}) has also been observed previously following TMA adsorption at room temperature on silica[17-19] and has been ascribed to the presence of $Al(CH_3)_{2(ads)}$. A similar assignment is made in this case. The presence of this surface species is in excellent agreement with the one-site Langmuir adsorption kinetics measured in UHV experiments on hydroxylated, oxidized alumina foil. Further corroboration of the presence of a dimethyl aluminum surface species will come from measurements of the amount of evolved methane and will be discussed in greater detail below.

The $Al(CH_3)_2$-covered surface is exposed to water and the data of Fig. 3 clearly indicate that carbon is reactively removed from the surface, presumably by reaction with the adsorbed aluminum dimethyl species. The peak positions in spectrum 7(b) of the gas evolved show the formation of CH_3D following exposure of the dimethylaluminum surface species to D_2O and confirms that this species reacts with water to yield methane, so that the plot of carbon removal as a function of exposure shown in Fig. 3 represents the kinetics of this removal process. It is evident from Fig. 3 that two kinetic steps, one fast below ~ 40 L exposure and one slow at higher exposures, are present in the reaction between water and the adsorbed dimethylaluminum. Assuming first-order reaction kinetics between the surface species and the gas-phase water gives:

$$-d\Theta/dE = k\Theta, \tag{3}$$

where Θ is the carbon coverage in the $Al(CH_3)_{2(ads)}$ species and is proportional to the carbon Auger signal, E is the water exposure, and k is a first-order rate constant. This can be simply integrated to give:

$$\Theta = \exp(-kE). \tag{4}$$

Assuming the presence of two removal rates yields:

$$\Theta = \Theta_1 \exp(-k_1 E) + \Theta_2 \exp(-k_2 E), \tag{5}$$

where Θ_1 and Θ_2 are the coverages of carbon present in each species corresponding to carbon removal rate constants k_1 and k_2, respectively. A fit to Eq. (5) is shown plotted as a solid line on the experimental data of Fig. 3 using $\Theta_1 = 0.51 \pm 0.04$, $k_1 = 0.12 \pm 0.01$ $Torr^{-1}$ s^{-1} and $\Theta_2 = 0.49 \pm 0.04$, $k_2 = 0.004 \pm 0.001$ $Torr^{-1}$ s^{-1}. The individual removal kinetics are indicated as dashed lines on Fig. 3. The fast reaction is ~ 30 times as fast as the slow rate at room temperature, and $\Theta_1/\Theta_2 = 1.05 \pm 0.15$; essentially equal amounts of carbon are removed in each of the two steps. Assuming an identical surface site density as used above (1×10^{15} cm^{-2}), the reaction probabilities per colliding water molecule can be calculated to give 0.25 for the probability corresponding to k_1, the fast rate, and 0.009 for k_2, the slow rate. That is $\sim 25\%$ of the incoming water molecules react in the first reaction, whereas only about 1% react in the second reaction. This latter probability is similar to that for TMA reacting with surface hydroxyl groups.

Note that since Θ_1 and Θ_2 are essentially equal, this implies that the first methyl group in the $Al(CH_3)_2$ surface species reacts rapidly, whereas the second group reacts approximately 30 times more slowly. Note also that addition of water to the dimethylaluminum-covered surface on high surface area alumina evolves an identical amount of methane as when TMA is initially added to the hydroxylated surface. This corresponds to the fast removal of surface carbon by reaction with water with rate constant k_1. The infrared spectrum of the resulting surface species, which has a stoichiometry $Al(CH_3)_1$, is shown in Fig. 6(a), and the corresponding expanded spectrum of the methyl region is shown in Fig. 7(c). This exhibits peaks at 2960, 2928, and 2856 cm^{-1}. The integrated intensity of this peak is approximately 50% of that of adsorbed dimethylaluminum in accord with the equimolar amounts of methane evolved by addition of TMA to hydroxylated alumina and by addition of water to this species.

The final adsorbed methyl group reacts with water to form further methane, leaving a hydroxylated surface but at a much slower rate than the first methyl group of the adsorbed dimethyl aluminum.

The experimental results can be summarized in the following proposed reaction scheme for the formation of an alumina film on an alumina substrate by the sequential reaction of TMA and water. The first step in the mechanism is the formation of hydrogen-bonded surface hydroxyl groups on alumina. This chemistry is well established on alumina surfaces using an array of techniques, primarily infrared spectroscopy.[22-28] This is proposed to react with TMA to yield a dimethyl aluminum surface species.

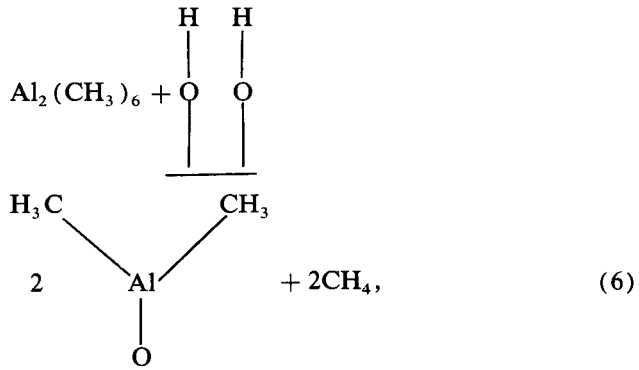

(6)

where, in this case, the TMA is written explicitly as a dimer,[59] so that 1 TMA dimer molecule reacts to form 2 methane molecules. This reaction step is in accord with the observation that TMA adsorbs via one-site Langmuir kinetics (Fig. 2), and the infrared spectrum is consistent with the presence of this surface species [Figs. 5(d) and 7(b)].

It is then proposed that a methyl group of the surface dimethylaluminum reacts with water (D_2O) (Fig. 3) with a reaction probability of $\sim 1\%$ evolving the CH_3D observed

in infrared spectroscopy [Fig. 6(b)] to leave behind a single surface CH_3. This final methyl group exhibits vibrational frequencies at 2960, 2928, and 2856 cm^{-1}. While this clearly can be assigned to CH_3 stretching vibrations, the exact nature of the surface species is unclear. A surface Al–O–CH_3 species has vibrational frequencies of 2550 and 2840 cm^{-1},[60] and so may partially account for the observed spectrum. Note that a Si–O–CH_3 group exhibits modes at 3000, 2960, and 2860 cm^{-1} [19] and so may account for the 2960 and 2900 cm^{-1} peaks in the spectrum of Fig. 7(c). The origin of the 2928 cm^{-1} peak remains unclear but might be due to a Al–CH_3 species. Note however that Si–CH_3 peaks are observed at 2960 and 2900 cm^{-1}.[17] This reaction yields the correct stoichiometry for the initial methane formation step following addition of TMA to hydroxylated alumina (2 CH_4) [Fig. 5; Eq. (6)] and after addition of D_2O (2 CH_3D) [Fig. 6(c)]. It also accounts for the observed decrease in carbon Auger signal (Fig. 3), the formation of CH_3D [Fig. 6(c)] and the surface infrared spectrum due to a surface CH_3 [Fig. 7(c)]. This reaction scheme is in accord with other pathways outlined for this process.[19,61] However, the last reaction step is likely to be complex since the initially three-coordinate aluminum will increase coordination on forming the oxide surface. It is also possible that an Al–O–Al bridge might be formed between two adjacent TMA-derived surface species during this reaction. It is of interest to note that in the case of an Al–N acid–base adduct, thermal decomposition results in the formation of a cubic Al–N framework structure.[62]

The remaining surface CH_3 can react with water, but with a much lower probability than the other methyl groups, to yield methane and hydroxylated alumina. The overall stoichiometry of the reaction steps outlined above corresponds to the equation:

$$Al_2(CH_3)_6 + 3H_2O \rightarrow Al_2O_3 + 6CH_4.$$

Since group III alkyls are Lewis acids[59] and water (and other group VI and group VII hydrides) are Lewis bases,[59] the initial reaction between water and a TMA-covered surface or between TMA and surface hydroxyl groups on alumina is likely to be the formation of a Lewis acid–base adduct. It has been shown that Lewis acid–base adducts comprising a group III alkyl and a hydrogen-containing donor molecule can thermally decompose via a reaction between the alkyl group and hydrogen to evolve an alkane.[63,64] It is likely that an analogous reaction pathway occurs in the case of adsorbed species on an alumina surface.

There are several pieces of evidence to show that alumina is indeed deposited at the surface during these experiments. In the case of high-surface-area alumina, the Al_2O_3 region of the spectrum is not substantially modified following several TMA + water deposition cycles. In addition, according to Figs. 8 and 9, both the absorbences and the light scattering increases as the number of deposition cycles increases indicating, first, that the pellet is becoming optically thicker and also that the average size of the particle is increasing. The increase in particle size can be roughly estimated from the results of the data shown in Figs. 8 and 9, assuming initially spherical particles. Since the light scattering cross section of a small particle is proportional to the particle volume V[56] then the decrease in intensity dI/dx can be written:

$$-dI/dx = k'VI. \tag{9}$$

Also, according to the Beer–Lambert law, the change in intensity due to light absorption is given by:

$$-dI/dx = \epsilon cI, \tag{10}$$

where ϵ is the extinction coefficient and c is the concentration. If the number of particles in the pellet remains constant and they have a volume V this equation can be written as:

$$-dI/dx = k''VI \tag{11}$$

and is essentially identical to Eq. 9. These can easily be integrated to give:

$$\ln(I/I_0) = -kVl \tag{12}$$

where l is the path length and k represents k' and k'', and Eq. 12 can be written:

$$A = kVl, \tag{13}$$

where A is the absorbance.

If the path length is taken to be approximately constant and the initial absorbance (due to scattering or absorption) is A_0 and the particle volume prior to the deposition is V_0 then:

$$A_0 = kV_0l. \tag{14}$$

If the absorbance changes by ΔA and the volume changes by ΔV, then:

$$\Delta A = k\Delta Vl, \tag{15}$$

so that when the radius of the particle changes due to film deposition by Δr and if the initial particle radius is r_0 and $\Delta r \ll r_0$:

$$\Delta A/A_0 = 3\Delta r/r_0. \tag{16}$$

If a film of uniform thickness is deposited by each cycle of TMA and water exposure, the particle radius will increase by an identical amount after each cycle and yield a linear plot of $\Delta A/A_0$ (for absorption) or $\Delta S/S_0$ (for light scattering) as a function of the number of deposition cycles as shown in the data of Figs. 8 and 9. Furthermore, according to equation 16 the slopes of these lines equals $3\,\Delta r/r_0$. These slopes are measured to be 0.18 ± 0.01 for infrared scattering and 0.12 ± 0.1 for infrared absorption. This indicates that the particle radius increases by between 4% and 6% following each cycle. The particle radius can be roughly estimated from the surface area (120 m^2/g) by assuming that they are spherical. This leads to an estimate of the particle diameter of ~40 Å, or $r_0 = 20$ Å. For $\Delta r/r_0 \sim 5\%$, this yields a value of film thickness deposited during each cycle of ~1 Å. This value corresponds well to that measured for alumina films deposited by sequential TMA and water doses in the technique known as ALE which has been measured at ~1 Å.[61]

The electron energy-loss spectrum [Fig. 4(d)] obtained following sequential TMA + water cycles exhibits low-energy loss features at 4, 14, 30, and 74 eV. This spectrum is broadly similar to that of the oxidized aluminum surface [Figs. 4(b) and 4(c)]. The features at higher loss energies are, however, absent. This implies that a surface film has

been deposited that is sufficiently thick that it obscures the features of the oxide layer below. The Auger spectrum at this stage exhibits only peaks due to oxygen and aluminum, and so must be ascribed to the presence of an oxide layer. One possible reason for the difference in loss spectra for the OMCVD-deposited layer [Fig. 4(d)] and that of the oxidized surface [Fig. 4(b)] may be that the former is disordered since it was grown at room temperature. It has been noted that the exciton loss energy is particularly sensitive to crystallinity in alumina so that for single-crystal α-alumina its loss energy is 9.5 eV[65] whereas for an oxidized foil, which is likely to be less crystalline than the single crystal, this value shifts to $\sim$8 eV (Ref. 50 and this work). The value of $\sim$4 eV measured for the OMCVD-deposited film at 300 K implies that the film is rather disordered.

V. CONCLUSIONS

It has been demonstrated that it is possible to grow thin films of alumina by the sequential application of TMA and water at room temperature both on high-surface-area alumina and in ultrahigh vacuum.

Both infrared spectroscopy and electron energy-loss spectroscopy (EELS) demonstrate that alumina films are deposited and that the particle radius increases by between 4% and 6%. The similarity in the reactions in each case allow the chemistry to be scrutinized in detail using infrared spectroscopy to identify surface intermediates on high-surface-area alumina and the reaction kinetics to be monitored in UHV.

A reaction mechanism is proposed which is in accord with all the experimental observations. Initially, adsorbed dimethyl aluminum is formed by reaction of gas-phase TMA with hydroxylated alumina. Further addition of water apparently reacts with a methyl group of the adsorbed dimethyl aluminum leaving an adsorbed, surface CH_3. The final methyl groups appear to react slowly, but eventually reacts with water to yield a hydroxylated alumina film.

[a] Author to whom correspondence should be addressed.

[1] *Gallium Arsenide, Materials, Devices, and Circuits*, edited by M. J. Howes and D. V. Morgan (Wiley, New York, 1985).
[2] H. M. Manasevit and W. I. Simpson, J. Electrochem. Soc. **116**, 1725 (1969).
[3] J.-P. Duchemin, M. Bonnet, F. Koelsch, and D. Huyghe, J. Cryst. Growth **45**, 181 (1978).
[4] S. D. Hersee and J.-P. Duchemin, Ann. Rev. Mater. Sci. **12**, 65 (1982).
[5] M. R. Leys and H. Veenvleit, J. Cryst. Growth **55**, 145 (1981).
[6] P. D. Dapkus, H. M. Manasevit, K. L. Hess, T. S. Low, and E. G. Stillman, J. Cryst. Growth **55**, 10 (1981).
[7] R. W. Glew, J. Physique C **5**, 281 (1982).
[8] G. B. Stringfellow, J. Cryst. Growth **68**, 111 (1984).
[9] S. P. Den Baars, B. Y. Maa, D. P. Dapkus, A. D. Danner, and H. C. Lee, J. Cryst. Growth **77**, 188 (1986).
[10] C. A. Larson, N. I. Buchanan, and G. B. Stringfellow, Appl. Phys. Lett. **52**, 480 (1988).
[11] H. Suzuki, K. Mori, M. Kawasaki, and H. Sato, J. Appl. Phys. **64**, 371 (1988).
[12] R. Luckerath, P. Tommack, A. Hertling, H. J. Koss, and P. Balk, J. Cryst. Growth **93**, 151 (1988).
[13] W. L Smith and T. Wartik, J. Inorg. Nucl. Chem. **29**, 629 (1967).
[14] A. W. Laubengayer and W. F. Gilliam, J. Am. Chem. Soc. **63**, 477 (1941).
[15] D. R. Biswas, C. Ghosh, and R. C. Layman, J. Electrochem. Soc. **130**, 234 (1984).
[16] *CRC Handbook of Chemistry and Physics*, edited by R. C. Weast (Chemical Rubber, Boca Raton, FL, 1981).
[17] J. B. Kinney and R. H. Staley, J. Phys. Chem. **87**, 3735 (1983).
[18] B. A. Morrow and R. A. McFarlane, J. Phys. Chem. **90**, 3192 (1986).
[19] D. J. C. Yates, G. W. Denbinski, W. R. Kroll, and J. J. Elliot, J. Phys. Chem. **73**, 911 (1969).
[20] B. A. Morrow, C. P. Tripp, and R. A. McFarlane, J. Chem. Soc., Chem. Commun. 1282 (1984).
[21] R. A. McFarland and B. A. Morrow, J. Phys. Chem. **92**, 5801 (1988).
[22] J. B. Peri and R. B. Hannan, J. Phys. Chem. **64**, 1526 (1960).
[23] J. B. Peri, J. Phys. Chem. **69**, 211 (1965).
[24] B. A. Hendrikson, D. R. Pearce, and R. Rudman, J. Catal. **24**, 82 (1972).
[25] J. K. Lee and S. W. Weller, Anal. Chem. **30**, 1057 (1966).
[26] H. P. Boehm, Adv. Catal., Rel. Subj. **16**, 179 (1966).
[27] J. G. Chen, J. E. Crowell, and J. T. Yates, Jr., J. Chem. Phys. **84**, 5906 (1986).
[28] J. Paul and F. M. Hoffmann, J. Phys. Chem. **90**, 5321 (1986).
[29] H. O. Pierson, Thin Solid Films **45**, 257 (1977).
[30] B. E. Bent, R. G. Nuzzo, and L. H. Dubois, Mat. Res. Soc. Symp. Proc. **101**, 177 (1988).
[31] Y. Rytz-Froidevaux, R. P. Salathe, and H. H. Gilgen Phys. Lett. A **84**, 216 (1981).
[32] L. H. Dubois, B. R. Zegarski, C.-T. Kao, and R. G. Nuzzo, Surf. Sci. **236**, 77 (1990).
[33] B. E. Bent, R. G. Nuzzo, and L. H. Dubois, J. Am Chem. Soc. **111**, 1634 (189).
[34] D. A. Mantell, Appl. Phys. Lett. **53**, 1387 (1988).
[35] R. B. Jackman and J. S. Foord, Surf. Sci. **201**, 47 (1988).
[36] J. R. Creigton, J. Electrochem. Soc. **136**, 271 (1989).
[37] R. B. Jackman and J. S. Foord, Surf. Sci. **209**, 151 (1989).
[38] F. Zaera, J. Vac. Sci. Technol. A **7**, 640 (1989).
[39] W. T. Tsang, J. Appl. Phys. **58**, 1415 (1985).
[40] W. T. Tsang, Appl. Phys. Lett. **45**, 1234 (1984).
[41] W. T. Tsang, Appl. Phys. Lett. **48**, 511 (1986).
[42] G. R. Larson and A. W. Sleight, Phys. Lett. A **28**, 203 (1968).
[43] J. Nishizawa and T. Kuribayashi, J. Electrochem. Soc. **132**, 51 (1985).
[44] A. Usui and H. Sunakawa, Jpn. J. Appl. Phys. **24**, L962 (1985).
[45] W. R. Salanek, R. Bergman, J.-E. Sundgren, A. Rackett, T. Motooka, and J. E. Green, Surf. Sci. **148**, 461 (1988).
[46] Y. Zhou, M. A. Henderson, and J. M. White, Surf. Sci. **221**, 160 (1989).
[47] J. E. Crowell, J. G. Chen, and J. T. Yates, Jr., Surf. Sci. **37**, 165 (1986).
[48] H. L Yu, M. C. Munoz, and F. Soria, Surf. Sci. **94**, L184 (1980).
[49] E. Johnson, Ph.D. thesis, Cornell University.
[50] J. Olivier and R. Poirier, Surf. Sci. **105**, 347 (1981).
[51] J. P. Maher and D. F. Evans, J. Chem. Soc., Chem. Commun. 5534 (1963).
[52] T. Ogawa, K. Hirota, and T. Miyazawa, Bull. Chem. Soc. Jpn. **38**, 1105 (165).
[53] G. Herzberg, *Molecular Spectra and Molecular Structure* (Van Nostrand Reinhold, New York, 1945), Vol. II.
[54] W. H. Bennett and C. F. Meyer, Phys. Rev. **32**, 888 (1928).
[55] A. Adel and E. F. Barker, J. Chem. Phys. **2**, 627 (1954).
[56] D. F. Eggers, N. W. Gregory, G. D. Halsey, and B. S. Rabinovitch, *Physical Chemistry* (Wiley, New York, 1964).
[57] G. S. Higashi and C. G. Feinberg, Appl. Phys. Lett. **55**, 1963 (1989).
[58] I. Langmuir, J. Am. Chem. Soc. **40**, 1361 (1918).
[59] F. A. Cotton and G. Wilkinson, *Advanced Inorganic Chemistry* (Interscience, New York, 1988).
[60] G. S. Higashi and L. J. Rothberg, J. Vac. Sci. Technol. B **3**, 1460 (1985).
[61] G. E. Coates and J. Graham, J. Chem. Soc., Chem. Commun. 233 (1963).
[62] O. T. Beachley, G. E. Coates, and G. Kohnstam, J. Chem. Soc., Chem. Commun. 3248 (1965).
[63] T. R. R. McDonald and W. S. McDonald, Proc. Chem. Soc. 382 (1963).
[64] E. T. Arakawa and M. W. Williams, J. Phys. Chem. Solids **29**, 735 (1968).
[65] R. G. Greenler, J. Chem. Phys. **37**, 2094 (1962).